ChemComm

Accepted Manuscript

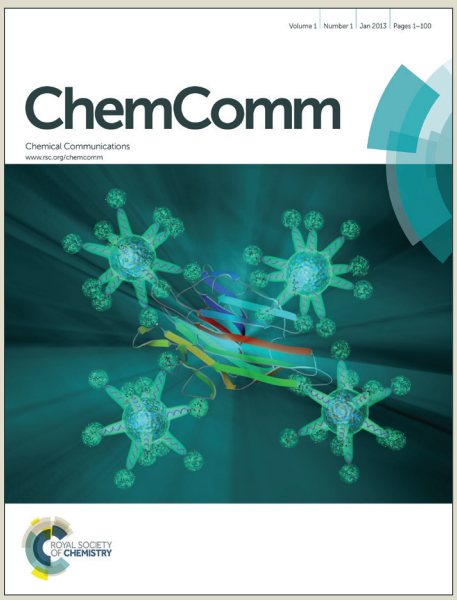

ROYAL SOCIETY OF CHEMISTRY

www.rsc.org/chemcomm

Cite this: DOI: 10.1039/c0xx00000x

www.rsc.org/xxxxxx

COMMUNICATION

Ag_2S-hollow Fe_2O_3 nanocomposites with NIR photoluminescence

Yingjie Chen,[a] Lifeng Dong,*[a,b] Mei Zhao[a] and Hongzhou Dong[a]

Received (in XXX, XXX) Xth XXXXXXXXX 20XX, Accepted Xth XXXXXXXXX 20XX
DOI: 10.1039/b000000x

A facile synthesis of Ag_2S-hollow Fe_2O_3 nanocomposites with NIR photoluminescence was firstly demonstrated by the sulfidation of Ag-Fe_2O_3 core-shell nanoparticles. Characteristic morphology transformations along with color changes were recorded and a mechanism was proposed for the sulfidation process, which can provide new possibilities to fabricate other complex nanostructures.

Synthesis of hybrid nanomaterials with controlled morphologies has gained considerable attention due to their potential multifunctional capabilities and tunable physical and chemical properties.[1-14] Along with the progress in nanomaterial synthesis, nanotemplated method has proven to be a powerful method for the topologically controlled synthesis of complex nanocomposites.[15,16] For example, Pt-CuS heteromers[17] and porous Pt-Co_xS nanoparticles[18] have been synthesized by the sulfidation of PtCu and PtCo alloys, while Au-Co_xS core-shell[18] and Pt-Ag_2S hollow-solid heterostructures[19] have been prepared with Au-Co and Ag-Pt core-shell nanotemplates. As to these alloy and bimetal nanotemplated approaches, the morphology of final products somewhat depended on the structure of the templates and different sulfidation reaction activities of components.[18-20] Similarly, a novel nanoreactor system with solid Fe_3O_4 and hollow Mn_3O_4 grains, possessing selective catalytic capacity and magnetic recoverability, has been fabricated with an etching process of preformed Fe_3O_4/MnO heteromers within silica nanoparticles.[21] Besides, hollow Fe_3O_4-ZnS nanocomposites, combining magnetic and optical functionalities, have been successfully synthesized with corrosion-aided Ostwald ripening of FeS core.[22] This kind of hybrid nanoparticles has shown the potential for simultaneous drug delivery, biomedical imaging and therapeutics. Nevertheless, autofluorescence background of living tissues has precluded conventional visible-emission nanocrystals from the application in most bioimaging *in vivo*. Thus, it is desirable to fabricate new kinds of multifunctional hybrid nanoparticles with interior void to solve autofluorescence problem.

As well known, nanoscale α-Ag_2S, with negligible toxicity and tunable near-infrared (NIR) photoluminescence, has attracted significant interest and attention for its superior properties over conventional organic dyes and NIR quantum dots for *in vivo* imaging.[23-25] Meanwhile, hollow iron oxide nanoparticles (QDs), with low toxicity and magnetic property, have attracted broad attentions for their great potential application as multifunctional agents for simultaneous magnetic resonance imaging (MRI) and drug delivery.[26] Hence, the integration of silver sulfide and hollow iron oxide into a nanosystem will lead to a novel kind of multifunctional hybrid nanoparticles, facilitating in vivo biomedical multitasking applications. Herein, we demonstrate a strategy for fabricating the nanocomposites of silver sulfide and hollow iron oxide by the sulfidation of Ag-Fe_2O_3 core-shell nanoparticles with 1-dodecanethiol (DDT) as surfactant and sulfur source. Color change along with the conversion of Ag-Fe_2O_3 core-shell nanoparticles into Ag_2S-Fe_2O_3 containing cage-bell and hollow nanostructures were observed and recorded. The consequently produced silver sulfide-hollow iron oxide nanocomposites showed broad NIR photoluminescence. A mechanism based on oxidation of Ag core and nucleation of Ag_2S nanocrystal on the outer surface of Fe_2O_3 shell was proposed for the observed morphological transformation process, which will help to understand the evolution process and design other complex nanostructures.

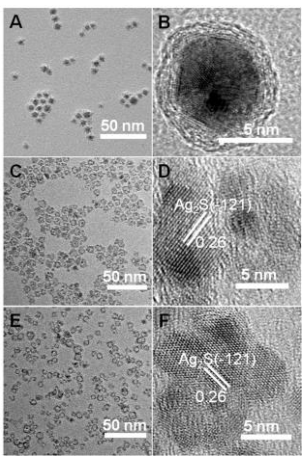

Fig. 1 TEM and high resolution TEM images of the preformed Ag-Fe_2O_3 core-shell nanoparticles (A, B) and the particles reacted with DDT at 80 °C for 1 h (C, D) and 2 h (E, F).

In our experiment, Ag-Fe_2O_3 core-shell nanoparticles were firstly synthesized by a seed-mediated growth method reported previously.[27] The morphological evolution of hybrid nanostructures during the sulfidation process with DTT was revealed by transmission electron microscopy (TEM) characterizations. As shown in Fig. 1, as-preformed Ag-Fe_2O_3 nanoparticles had uniform core-shell nanostructures with ~3.5 nm core and ~2 nm Fe_2O_3 shell. These nanocomposites transformed from core-shell (Fig. 1 A, B) to cage-bell (Fig. 1 C,

D) and the final hollow nanostructures (Fig. 3 E, F) along with the sulfidation reaction time. Compared with Ag-Fe_2O_3 core-shell nanoparticles, a gradual contrast decrease in the core domain and emerging decoration on the outer shell were observed during the sulfidation process, indicating the diminishing of Ag cores and an accompanying appearance and growth of Ag_2S nanocrystals on the outer surface of the iron oxide shell. Thus, Ag_2S-cage-bell-Ag-Fe_2O_3 nanostructures were formed prior to the formation of Ag_2S-hollow Ag-Fe_2O_3 nanocomposites, the diameter and morphology of whose hollow voids fabricated by sulfidation treatment were consistent with initial Ag cores, suggesting that the removal of the Ag core from the core–shell nanoparticles did not collapse the particle geometry. The measured lattice spacing of ~0.26 nm for the nanocrystals decorated on the outer shell could be indexed as (-121) facet of monoclinic-Ag_2S (JCPDS 14-0072). The EDS line scan for Ag-Fe_2O_3 core-shell and Ag_2S-hollow Fe_2O_3 nanocomposites further revealed the diffusion of Ag from the core to the outer surface of Fe-O containing shell (Fig. S1). X-ray diffraction (XRD) experiments confirm the sulfidation of Ag nanocrystals into Ag_2S nanoparticles in the hybrid nanoparticles. The XRD peaks for Ag nanocrystals vanished after the sulfidation reaction with DDT, while the broadening of those peaks for Fe_2O_3 showed the appearance of monoclinic-Ag_2S (JCPDS 14-0072) (Fig. S2).

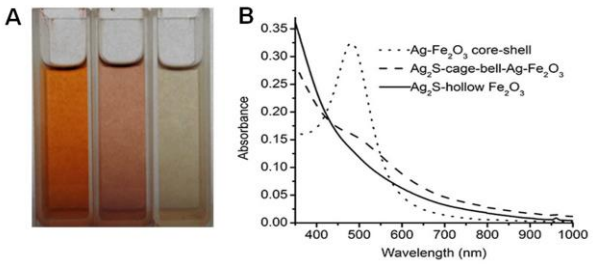

Fig. 2 Photographs of Ag-Fe_2O_3 core–shell, Ag_2S-cage-bell-Ag-Fe_2O_3 and Ag_2S-hollow Fe_2O_3 nanoparticles dispersed in hexane (A: from left to right) and their UV-Vis-NIR absorption spectra (B).

Along with the reaction of DDT and Ag-Fe_2O_3 core-shell nanoparticles in octadecene (ODE) at 80 °C, the solution color slowly changed from brown-red to dark-red and finally dark-brown (Fig. 2 A), standing for different sulfidation progresses. UV-Vis-NIR absorption spectra of nanocomposites corresponding to the three steps were shown in Fig. 2 B. The characteristic red-shift surface plasmon resonance peak of Ag nanoparticles at 500 nm gradually diminished from the initial core-shell templates to cage-bell and hollow nanocomposites, while a shoulder peak in the NIR window emerged due to the low-energy excitonic absorption of Ag_2S nanocrystals. As-synthesized Ag_2S-hollow Fe_2O_3 nanocomposites showed an obvious absorption peak at 960 nm (Fig. 3 A), the corresponding NIR photoluminescence spectrum of which showed a major emission peak at around 1100 nm and three shoulder emission peaks near 1000 nm, 1250 nm and 1300 nm, respectively (Fig. 3 B). According to the size-dependent excited state optical properties of Ag_2S nanocrystals, the concomitance of several emission peaks in the NIR window can be explained by the presence of inhomogeneous size of Ag_2S NPs in the nanocomposites. The PL quantum yield (2.8%) and photostability of nanocomposites were determined against indocyanine green (ICG) in DMSO (QY = 13%). The nanocomposites retained 73% of original fluorescence after 60 min continuous illumination with mercury lamp, whereas the organic NIR fluorescent ICG decreased to 46% (Fig. S3). Meanwhile, the corresponding saturation magnetization values of Ag-Fe_2O_3 core-shell and Ag_2S-hollow Fe_2O_3 nanocomposites were 8.0 and 10.3 emu/g, respectively (Fig. S4). Since there were bound to loss of Ag ions from nanoparticles into solution containing dissociative DDT, so the even higher magnetic property of nanoparticles after sulfidation should be due to the higher weight loss for Ag diffusion than weight increase for Ag_2S formation.

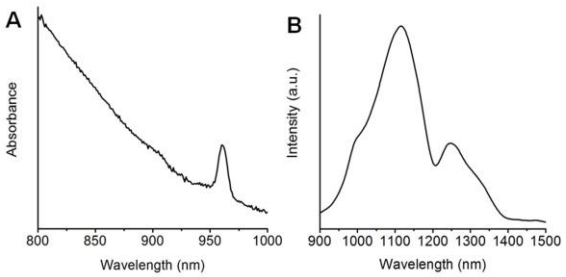

Fig. 3 NIR absorption spectrum (A) and photoluminescence (PL) spectrum (B) of Ag_2S-hollow Fe_2O_3 nanocomposites in n-hexane at room temperature under λ_{ex}=960 nm.

It worths noting that oxygen played an important role in the sulfidation of Ag-Fe_2O_3 by DDT. Under the protection of nitrogen, Ag-Fe_2O_3 core-shell nanoparticles dispersing in the mixture of DDT and ODE showed their stability at 80 °C. Their characteristic color retained brown red even after 3 h. The similar role of air in the sulfidation of metal-containing template by DDT has also been reported by Jiang and co-workers[23], which was explained by an oxidation, *in situ* formation of metal thiolate, and subsequent decomposition mechanism for the formation of metal sulfide-containing heteromers. Meanwhile, characteristic peaks for the stretching vibration of C-S at 600-700 cm^{-1} were found in both FTIR spectra of DDT and Ag_2S-hollow Ag-Fe_2O_3 nanocomposites, while a weak S-H stretching vibration at 2550-2600 cm^{-1} was found only in the FTIR spectrum of DDT (Fig. 4).[28] The presence of the C-S stretching vibration and disappearance of the S-H stretching vibration indicated the capping of DDT on the surface of nanoparticles by the S atom anchoring.[29]

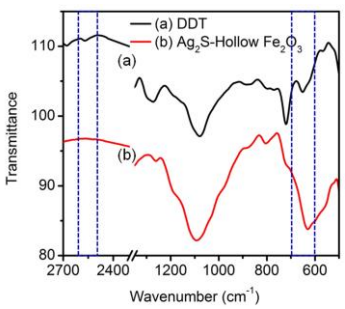

Fig. 4 FTIR spectra of (a) DDT and (b) Ag_2S-hollow Fe_2O_3 nanoparticles.

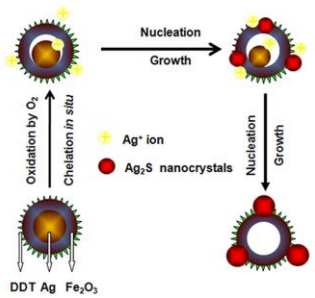

Scheme 1 Proposed mechanism for the sulfidation of Ag-Fe_2O_3 core-shell nanoparticles by DDT with progress time.

Thus, this sulfidation process of hybrid nanocomposites from core-shell to cage-bell and hollow structures was illustrated in Scheme 1. The Ag core shielded by Fe_2O_3 shell had no surface molecular binding and was easily etched by the oxidation of O_2. The resulting Ag^+ ions released by Ag core slowly diffused out of Fe_2O_3 shell and chelated with outer surfactant DDT *in situ*. These chelated complexes gradually decomposed into Ag_2S nanocrystals and anisotropically nucleated on the outer surface of Fe_2O_3 shell to form cage-bell nanocomposites. These Ag_2S nucleus incidentally grew with the continued oxidation and shrinkage of Ag cores, resulting in hollow Fe_2O_3 nanostructures decorated with Ag_2S. The concurrence of Ag oxidation, Ag^+ diffusion, Ag^+-DDT formation and decomposition made the sulfidation process adjustable by regulating reaction temperature and proportion between nanotemplates and DDT. High temperature accelerates Ag oxidation, Ag^+ diffusion, decomposition of silver thiolates (Fig S5), while more DDT promotes the extraction of Ag^+ ions from the shell and the formation of dissociative Ag^+-DDT (Fig S6).

Conclusions

We have demonstrated a facile strategy for the fabrication of Ag_2S-hollow Fe_2O_3 nanostructures based on the sulfidation of Ag-Fe_2O_3 core-shell nanoparticles with 1-dodecanethiol (DDT) as surfactant and sulfur source. Morphology transformation along with the color change from Ag-Fe_2O_3 core-shell nanoparticles to Ag_2S-Fe_2O_3 containing cage-bell and hollow nanostructures were characterized and recorded. The consequently produced silver sulfide-hollow iron oxide nanocomposites showed broad NIR photoluminescence. A mechanism based on oxidation of Ag in Ag-Fe_2O_3 core-shell nanoparticles, inside-out diffusion and *in situ* chelate of Ag^+, and nucleation and growth of Ag_2S nanocrystal on the outer surface of the Fe_2O_3 shell was proposed, which will help design and fabricate other complex nanostructures.

This work was partially supported by the International Science & Technology Cooperation Program of China (2014DFA60150), the National Natural Science Foundation of China (51172113), the Taishan Scholar Overseas Distinguished Professorship program, and the Shandong Natural Science Foundation (JQ201118).

Notes and references

[a] *College of Materials Science and Engineering, Qingdao University of Science and Technology, Qingdao 266042, China. Fax/Tel: 86-532-84022869; E-mail: DongLifeng@qust.edu.cn*
[b] *Department of Physics, Astronomy, and Materials Science, Missouri State University, Springfield, MO 65897, USA. Fax: 1-4178366226; Tel: 1-4178363755; E-mail: LifengDong@MissouriState.edu*

† Electronic Supplementary Information (ESI) available. See DOI: 10.1039/b000000x/

1 E. S. Shibu, K. Ono, S. Sugino, A. Nishioka, A. Yasuda, Y. Shigeri, S.-i. Wakida, M. Sawada and V. Biju, *ACS Nano*, 2013, **7**, 9851-9859.
2 Q. Tian, J. Hu, Y. Zhu, R. Zou, Z. Chen, S. Yang, R. Li, Q. Su, Y. Han and X. Liu, *Journal of the American Chemical Society*, 2013, **135**, 8571-8577.
3 J. Yang, D. Shen, L. Zhou, W. Li, X. Li, C. Yao, R. Wang, A. M. El-Toni, F. Zhang and D. Zhao, *Chemistry of Materials*, 2013, **25**, 3030-3037.
4 Y. Sun, M. Chen, Z. Wang and L. Wu, *Chemical Communications*, 2014, **50**, 5767-5770.
5 X. Liu, C. Lee, W.-C. Law, D. Zhu, M. Liu, M. Jeon, J. Kim, P. N. Prasad, C. Kim and M. T. Swihart, *Nano Letters*, 2013, **13**, 4333-4339.
6 D. Nepal, L. F. Drummy, S. Biswas, K. Park and R. A. Vaia, *ACS Nano*, 2013, **7**, 9064-9074.
7 H. Liu, J. Qu, Y. Chen, J. Li, F. Ye, J. Y. Lee and J. Yang, *Journal of the American Chemical Society*, 2012, **134**, 11602-11610.
8 J. Xie, F. Zhang, M. Aronova, L. Zhu, X. Lin, Q. Quan, G. Liu, G. Zhang, K.-Y. Choi, K. Kim, X. Sun, S. Lee, S. Sun, R. Leapman and X. Chen, *ACS Nano*, 2011, **5**, 3043-3051.
9 S. Shen, Y. Zhang, L. Peng, Y. Du and Q. Wang, *Angewandte Chemie*, 2011, **123**, 7253-7256.
10 J. Yang and J. Y. Ying, *Chemical Communications*, 2009, 3187-3189.
11 T.-T. Zhuang, F.-J. Fan, M. Gong and S.-H. Yu, *Chemical Communications*, 2012, **48**, 9762-9764.
12 A. Walther and A. H. E. Müller, *Chemical Reviews*, 2013, **113**, 5194-5261.
13 N. C. Bigall, W. J. Parak and D. Dorfs, *Nano Today*, 2012, **7**, 282-296.
14 C. d. M. Donega, *Chemical Society Reviews*, 2011, **40**, 1512-1546.
15 M. H. Oh, T. Yu, S.-H. Yu, B. Lim, K.-T. Ko, M.-G. Willinger, D.-H. Seo, B. H. Kim, M. G. Cho, J.-H. Park, K. Kang, Y.-E. Sung, N. Pinna and T. Hyeon, *Science*, 2013, **340**, 964-968.
16 S.-U. Lee, J. W. Hong, S.-I. Choi and S. W. Han, *Journal of the American Chemical Society*, 2014, **136**, 5221-5224.
17 X. Ding, Y. Zou, F. Ye, J. Yang and J. Jiang, *Journal of Materials Chemistry A*, 2013, **1**, 11880-11886.
18 D. Wang, X. Li, H. Li, L. Li, X. Hong, Q. Peng and Y. Li, *Journal of Materials Chemistry A*, 2013, **1**, 1587-1590.
19 H. Liu, F. Ye, H. Cao, G. Ji, J. Y. Lee and J. Yang, *Nanoscale*, 2013, **5**, 6901-6907.
20 X. Ding, Y. Zou and J. Jiang, *Journal of Materials Chemistry*, 2012, **22**, 23169-23174.
21 K. S. Lee, R. M. Anisur, K. W. Kim, W. S. Kim, T.-J. Park, E. J. Kang and I. S. Lee, *Chemistry of Materials*, 2012, **24**, 682-687.
22 Z. Wang, L. Wu, M. Chen and S. Zhou, *Journal of the American Chemical Society*, 2009, **131**, 11276-11277.
23 P. Jiang, Z.-Q. Tian, C.-N. Zhu, Z.-L. Zhang and D.-W. Pang, *Chemistry of Materials*, 2011, **24**, 3-5.
24 Y. Du, B. Xu, T. Fu, M. Cai, F. Li, Y. Zhang and Q. Wang, *Journal of the American Chemical Society*, 2010, **132**, 1470-1471.
25 G. Chen, F. Tian, Y. Zhang, Y. Zhang, C. Li and Q. Wang, *Advanced Functional Materials*, 2014, **24**, 2481-2488.
26 T. Chen, M. I. Shukoor, R. Wang, Z. Zhao, Q. Yuan, S. Bamrungsap, X. Xiong and W. Tan, *ACS Nano*, 2011, **5**, 7866-7873.
27 Y. Chen, N. Gao and J. Jiang, *Small*, 2013, **9**, 3242-3246.
28 S. Shen, Z. Tang, Q. Liu and X. Wang, *Inorganic Chemistry*, 2010, **49**, 7799-7807.
29 M. Deng, S. Shen, X. Wang, Y. Zhang, H. Xu, T. Zhang and Q. Wang, *CrystEngComm*, 2013, **15**, 6443-6447.